

The regeneration of stellar bars by tidal interactions. Numerical simulations of fly-by encounters.

I. Berentzen^{1,2*}, E. Athanassoula², C.H. Heller³, and K.J. Fricke¹

¹Universitäts-Sternwarte, Geismarlandstraße 11, D-37083 Göttingen, Germany

²Observatoire Astronomique de Marseille-Provence, 2 Place Le Verrier, F-13248 Marseille Cedex 4, France

³Georgia Southern University, Department of Physics, Statesboro, GA 30460, U.S.A.

22 March 2018

ABSTRACT

We study the regeneration of stellar bars triggered by a tidal interaction, using numerical simulations of either purely stellar or stellar+gas disc galaxies. We find that interactions which are sufficiently strong to regenerate the bar in the purely stellar models do not lead to a regeneration in the dissipative models, owing to the induced gas inflow in those models. In models in which the bar can be regenerated, we find a tight correlation between the strength and the pattern speed of the induced bar. This relation can be explained by a significant radial redistribution of angular momentum in the disc due to the interaction, similar to the processes and correlations found for isolated barred spirals. We furthermore show that the regenerated bars show the same dynamical properties as their isolated counterparts.

Key words: galaxies: evolution – galaxies: interactions – galaxies: structure – galaxies: kinematics and dynamics.

1 INTRODUCTION

Barred galaxies amount to more than one third of the catalogued disc galaxies in optical wavelengths (e.g., de Vaucouleurs 1963) and to about two thirds in the near-infrared (Eskridge et al. 2000). It has been established by now, that the *life* of a bar can be divided into several episodes: its formation, evolution, dissolution and maybe its regeneration (e.g., see review by Friedli 1999).

Two mechanisms for the formation of bars in disc galaxies are being widely accepted at present. Bar formation can occur, as shown in many numerical simulations, spontaneously by a global instability in cold, rotationally supported stellar discs (e.g., Miller, Prendergast & Quirk 1970; Hohl 1971; Ostriker & Peebles 1973; Sellwood 1981; Athanassoula & Sellwood 1986; etc.). The second mechanism, also confirmed in numerous *N*-body simulations, is the formation of tidally induced bars, triggered by interactions with neighbouring galaxies (e.g., Byrd et al. 1986; Noguchi 1987, 1988, 1996; Gerin, Combes & Athanassoula 1990; Barnes & Hernquist 1991; Salo 1991; Miwa & Noguchi 1998; etc.). To distinguish between the two bar forming mechanisms, Miwa & Noguchi (1998) compared the properties of spontaneously formed and tidally induced bars by means of *N*-body simulations and argued that tidally induced bars are slow ro-

tators, while the spontaneously formed bars have usually higher pattern speeds.

Athanassoula (2003) argued that the evolution of bars in isolated disc galaxies is driven by the redistribution of angular momentum. Since this is crucial for the work presented here, we will briefly summarise the main results. Disc galaxies strive to transfer angular momentum outwards (Lynden-Bell & Kalnajs 1972). Disc material in the inner disc, being at resonance with the bar, emits angular momentum to resonant material in the outer disc, or in the spheroidal components like the halo and the bulge (Athanassoula 2002). The corotation radius of the bar roughly divides the regions of disc emitters from that of disc absorbers. The size and the pattern speed of the bar responds to the angular momentum exchange in a way as to keep an equilibrium between the emitters and absorbers. These recent results argue strongly that the strength and the pattern speed of the bar are determined by the amount of angular momentum exchanged. The bar’s slowdown rate found in numerical simulations depends on the relative halo mass and on the velocity dispersion of both the disc and the halo. Furthermore, Athanassoula (2002) has shown that bar growth in the disc can be stimulated even in massive halos due to the destabilising influence of resonant stars in the halo.

Another factor influencing the evolution of bars is the interstellar medium in the disc. Owing to the gravitational

* Email: iberent@uni-sw.gwdg.de

torques of the bar, gas can be driven towards the centre of the galaxy and this is likely to be accompanied by central starbursts and formation/fueling of an active galactic nucleus (Shlosman, Frank & Begelman 1989). Fully self-consistent numerical simulations including gas have shown that substantial gas inflow can weaken significantly, or even destroy, the bar (Friedli & Benz 1993; Berentzen et al. 1998). The central mass concentrations and the times-scales found in these simulations, however, might be too high and too short, respectively, to be in agreement with the relatively high fraction of barred galaxies observed. Furthermore, this fraction seems to be independent of galaxy morphology, i.e. the same in early- and late-type disc galaxies, while early-types are known to have considerably less gas.

A regeneration of the stellar bar, i.e. a secondary episode of bar-formation during the lifetime of the disc, has been suggested as a possible mechanism to explain the observed number of barred galaxies. One scenario for this (Sellwood & Moore 1999; Bournaud & Combes 2002) could be the accretion of gas-rich companion galaxies or freshly infalling gas, which, by adding colder material to the disc, may cool it sufficiently and allow the generation of a new bar. Another scenario suggested, and upon which we will focus in this paper, could be the regeneration of a previously dissolved or weakened bar by a tidal encounter with a neighbouring galaxy. In this work we study this regeneration process by means of fully self-consistent, 3D numerical simulations. The host galaxy, in which the first, i.e. spontaneously formed, bar has significantly weakened before the interaction, is tidally perturbed by a companion galaxy. Various orbits and masses have been considered for the companion, in order to cover a wide parameter space. We provide a comparison between pure stellar and two-component stars+gas models and describe the regeneration process and the dynamical properties of the tidally induced bars.

In §2 we describe the numerical methods and the initial conditions of the galaxy models. The evolution and the dynamical properties of the isolated models with and without gas are described in §3 and §4, respectively. In §5 and §6 we present the results of the interacting models with and without gas, respectively. The results are then discussed in §7 and finally we give a summary in §8.

2 NUMERICAL METHODS AND INITIAL CONDITIONS

2.1 Methods

To evolve both the collisionless component, representing the stars and the dark matter, and the dissipative component, representing the gas, we use an N -body algorithm, combined with a smoothed particle hydrodynamics (hereafter SPH) algorithm (e.g., review by Monaghan 1992). For this purpose we use the version of the hybrid N -body/SPH code of Heller (1991; see also Heller & Shlosman 1994). The fully self-consistent 3D algorithm employs such features as a spatially varying smoothing length, a hierarchy of time-bins to approximate individual time-steps, a viscosity “switch” to reduce the effects of viscous shear, and the special-purpose hardware GRAPE-3AF to compute the gravitational forces and neighbour interaction lists (Sugimoto et al. 1990; Steinmetz 1996).

Table 1. Initial model parameters.

Component	Type	N_d	M_d	a_d	r_{cut}	z_0
Disc – I0						
stars	KT	13 500	0.54	1.0	5.0	0.20
gas	KT	10 000	0.16	1.0	5.0	0.05
Disc – I1						
stars	...	17 500	0.7
Component	Type	N_h	M_h	b_h	r_{cut}	
Halo						
stars	Pl	32 500	1.30	5.0	10.0	...
Component	Type	N_c	M_c			
Companion						
C1	pt	1	2.0
C2	pt	1	4.0
C3	pt	1	6.0
C4	pt	1	8.0
C5	pt	1	0.66
C6	pt	1	1.0

2.2 Initial conditions

Our isolated model I0 is initially composed of a stellar and a gaseous disc, embedded in a spherical halo. The radial surface density of both the discs follows a truncated Kuzmin-Toomre (hereafter KT) profile (Kuzmin 1956; Toomre 1963) with a radial scalelength a_d . Their vertical density profile follows the sech^2 distribution of an isothermal sheet (Spitzer 1942). The halo is set up initially as a Plummer (hereafter Pl) sphere (Plummer 1911) with a radial scalelength b_h , and is then allowed to relax in the gradually introduced potential of the *frozen* disc. For a detailed description of the initial model I0 see also Berentzen et al. (2003). The initial model parameters are summarised in Tab. 1. The columns from left to right give the component, the type of density profile, the particle number, the total mass, the radial scalelengths a_d and b_h , the cut-off radius r_{cut} , and the vertical scaleheight z_0 of each component. Our isolated model I1 differs from model I0 in that about one third of the gas particles have been replaced with stellar particles, i.e. with keeping their positions and assigning new masses, keeping the total disc mass the same as in model I0. The remaining gas particles have been completely removed from the disc. We then assign velocities to the new stellar particles according to the mean velocity distribution of the *old* underlying stellar disc. Both host galaxies, I0 and I1, are evolved in isolation first. The disc of I0 is constructed so as to be globally unstable to non-axisymmetric perturbations and form a large-scale bar. Owing to induced gas-inflow, the stellar bar in model I0 weakens significantly during its evolution, but is present in both models before the companion galaxy is introduced.

The companion galaxy in the interaction simulations is represented by a smoothed point mass (hereafter pt) for simplicity, applying a Plummer softening for the force calculation. Since the GRAPE-3 hardware can only handle a fixed softening length, we apply the same softening for all particles, including the companion. The mass ratio $M_{\text{host}} : M_{\text{comp}}$,

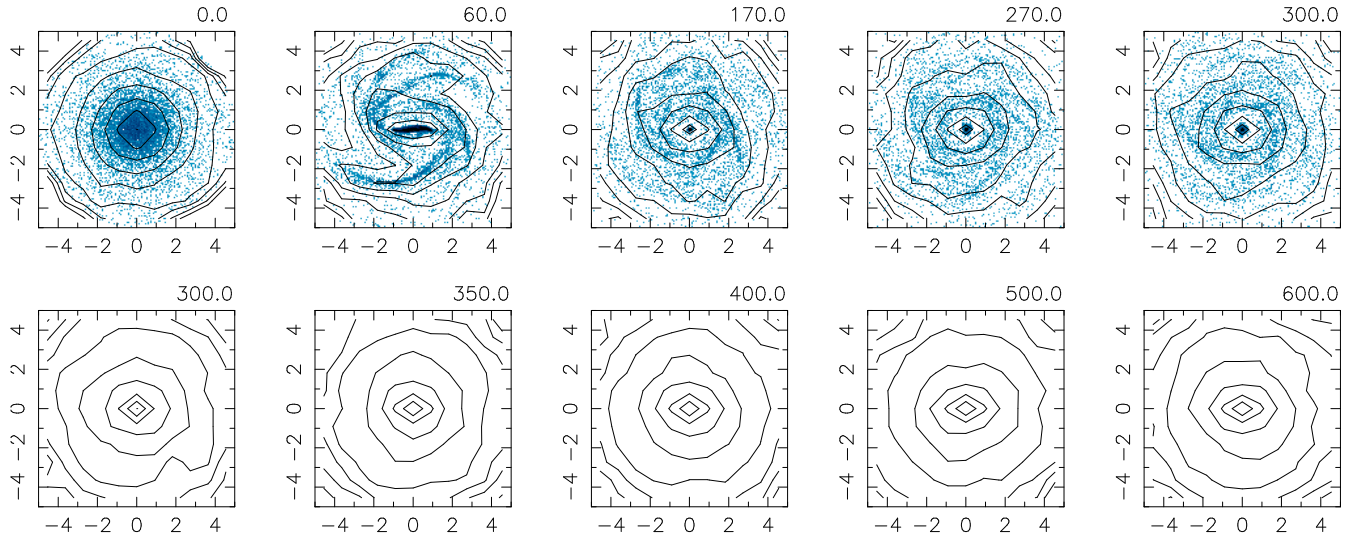


Figure 1. Evolution of the isolated models. We show the face-on isodensity contours of the stellar disc for models I0 (upper panels) and I1 (lower panels) and a grey-scale density plot of the gas particle distribution for model I0. The disc rotation is counter-clockwise, and the disc has been rotated in each frame so that the bar is oriented along the x -axis. We give the time on the top of each panel. Time and length scales are both in computer units.

where M_{host} and M_{comp} are the total mass of the host and of the companion galaxy, respectively, has been varied between 1:1 to 1:4. In addition a few simulations have been run with less massive companions. For the simulations presented in this paper we confine ourselves to planar fly-by encounters, i.e. the orbits of the host and the companion galaxy are unbound and lie in the equatorial plane of the host. The initial conditions have been chosen such as to provide a strong perturbation to the disc. The orbit of the companion galaxy is prograde with respect to the rotation in the host disc and has been chosen to be either parabolic or hyperbolic, with different pericentric separations R_{peri} . The pericentric position has been chosen such that at time of pericentre (hereafter t_{peri}) the major axis of the relatively weak bar, which has formed/evolved in the hosts disc before the encounter, points towards the companion. The times of pericentric separation have been chosen to be $t_{\text{peri}} = 270$ and 500 for all simulations with host galaxy I0 and I1, respectively. The initial orbital parameters at t_{peri} have been calculated from the solution of the corresponding two-body problem, either for a given orbital eccentricity e , or for a pericentric angular frequency of the companion

$$\omega_{\text{peri}} = v_{\text{peri}}/R_{\text{peri}}, \quad (1)$$

where v_{peri} is the velocity of the companion at pericentre. To obtain the initial centre of mass positions and velocities of the host and of the companion galaxy, we integrate their orbits backward in time, starting from the pericentric time t_{peri} , until the distance ΔR between host and companion is roughly 10 times the cut-off radius of the initial halo. During this backwards orbit integration the particles of the host are frozen with respect to each other. Owing to the limited spatial range of the GRAPE-3 hardware, the interaction models have been calculated in the inertial frame of the host galaxy and the force of the companion has partly been calculated by direct summation on the front-end, i.e. without using the GRAPE hardware.

2.3 Units

The adopted units for mass, distance, and time are $M = 6 \times 10^{10} M_{\odot}$, $R = 3 \text{ kpc}$ and $\tau = 10^7 \text{ yr}$, respectively, for which the gravitational constant G is unity. The dynamical time is $\tau_{\text{dyn}} \equiv (r_{1/2}^3/G M_{1/2})^{1/2} = 4.8 \times 10^7 \text{ yr}$, where $M_{1/2}$ is half the total mass of the host and $r_{1/2}$ is its half-mass radius, which is, after relaxation of the halo, approximately 8.5 kpc or in terms of the disc scalelength, $2.8 a_{\text{d}}$. The initial stellar disc rotation period in these units then corresponds to $t_{\text{rot}} \equiv 2\pi\tau_{\text{dyn}} \approx 3 \times 10^8 \text{ yr}$. A fixed gravitational softening length of $\epsilon = 0.375 \text{ kpc}$ is used for all particles. An isothermal equation of state is used for the gas with a sound speed of $v_{\text{s}} = 12 \text{ km s}^{-1}$. The corresponding thermal gas temperature is 10^4 K .

3 ISOLATED MODEL WITH GAS – MODEL I0

As described in the previous section, the isolated galaxy model I0 is composed of a stellar (collisionless) and a gaseous (dissipative) disc component, embedded in a *live* halo. The morphological evolution of the disc is shown in Fig. 1 (upper panels). The stellar disc has been chosen to be initially bar unstable and forms a large-scale bar within roughly $2 t_{\text{rot}}$. The stellar bar reaches its maximum strength at about $t = 60$ (see Fig. 2). The bar strength, here defined by the normalized $m = 2$ Fourier component of the stellar disc mass distribution, has been measured inside a cylindrical radius of $R = 1.25$ and about one scaleheight of the disc plane. Owing to the torque of the bar, most of the gas in the bar region is driven towards the centre of the galaxy, accumulating in a nuclear and circumnuclear disc. At the end of the run the mass of the gaseous nuclear disc represents some 18 per cent of the total mass within a spherical radius of 1.0 kpc. As a result of the growing central mass concentration the stellar bar weakens significantly, and the disc settles down in a quasi-stable state at about $t \approx 120$. Some gas also accumu-

lates near the end of the weak stellar bar, forming an oval ring close to the position of the inner ultra-harmonic resonance (hereafter UHR) at $R=2.25$ kpc. The pattern speed of the bar (hereafter Ω_p) first increases due to the short burst of gas inflow and thereafter reaches a constant rate of about $\Omega_p=0.3\tau^{-1}$, or $29.3\text{ km s}^{-1}\text{ kpc}^{-1}$. The evolution of model I0 is followed in total up to $t=300$, i.e. about 10 disc rotations. A more detailed description of the evolution of this model and its dynamical properties is given in Berentzen et al. (2003).

To identify the presence and the location of the main planar resonances in the disc, we apply both the linear (epicyclic) approximation and non-linear methods. We therefore calculate the gravitational potential in the $z=0$ plane of the disc on a Cartesian grid and symmetrise it with a four-fold symmetry with respect to the main axes of the bar. From the potential we then derive the azimuthally averaged circular and epicyclic frequency $\Omega_c(R)$ and $\kappa(R)$, respectively. The standard linear resonance condition is given by

$$\Omega_p = \Omega_c + \frac{l}{m} \kappa, \quad (2)$$

with integers l and m . For a strict definition of the inner Lindblad resonances (hereafter ILRs; with $l=-1$ and $m=2$) three extensions to the linear definition have been proposed (see Athanassoula (2003) for a discussion), which are not fully compatible to each other and sometimes in contradiction. Throughout this work, unless otherwise noted, we apply the orbital structure definition for the ILRs, i.e. by saying that an ILR exists if and only if the x_2 and x_3 orbit families exist. The ILRs have been confirmed in this case by calculating the surfaces of section (hereafter SOS). The SOS have been constructed by integrating orbits of a given Jacobian energy (hereafter E_J ; see also Sec. 4) in the equatorial plane of the disc and marking the points in the (y, \dot{y}) plane each time the orbits cross the line $x=0$ with $\dot{x} < 0$ (e.g., Binney & Tremaine 1987). At the end of the run ($t=300$) the corotation radius (hereafter CR; i.e., the radius at which $\Omega_c=\Omega_p$) in this model is at about 6.15 kpc ($E_J \approx -0.91$), and the ILRs are located at about 0.47 kpc (inner ILR; $E_J = -1.58$) and 2.1 kpc (outer ILR; $E_J = -1.10$), respectively.

4 ISOLATED MODEL WITHOUT GAS – MODEL I1

We study the regeneration of the bar by interactions of two different types of host galaxies – with and without gas in the disc – which, nevertheless, have similar dynamical properties. We therefore construct our purely stellar model I1 by replacing the gas particles in model I0 with stellar particles, as described in Sec. 2.2. This has been accomplished for the last snapshot of model I0 at $t=300$, i.e. at the end of the run, when the amplitude of the initial bar has very considerably decreased and the disc is in a quasi-stable state. After replacing the gaseous particles with stellar ones we follow the evolution of the new model I1 for another $\Delta t=300$. The morphological evolution of the stellar disc is shown in Fig. 1 (lower panels), and in Fig. 2 we show the evolution of the bar strength and of the pattern speed. The bar strength first

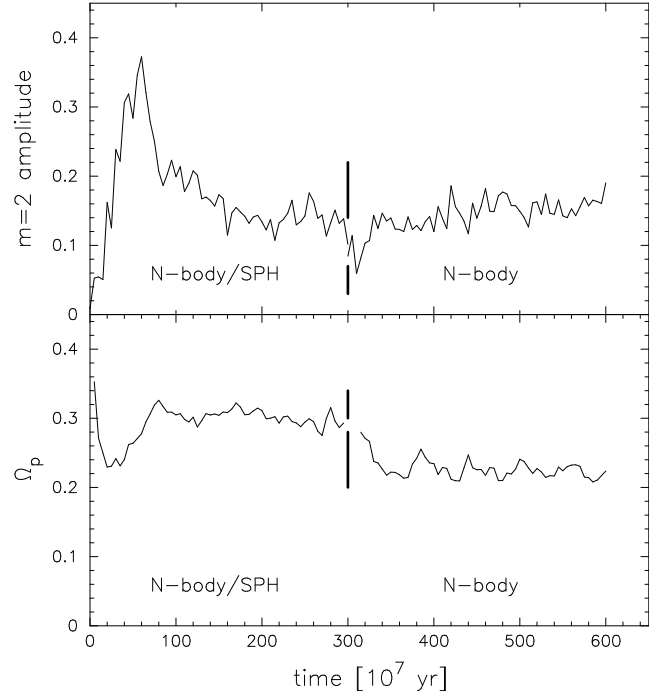


Figure 2. Evolution of the bar strength (upper panel) and pattern speed (lower panel) for models I0 (stars+gas) and I1 (stars). The transition between the two models is marked by two vertical dashes ($t=300$).

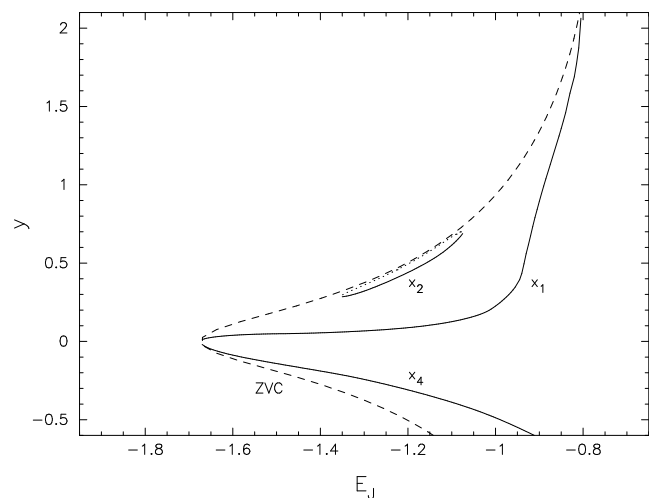


Figure 3. Characteristic diagram of the isolated model I1 at the end of the run. We show the characteristic curves of the main orbit families (full lines) and the zero velocity curve (ZVC; dashed line).

decreases abruptly, owing to the *newly* added stellar particles, which follow initially the distribution of the gas. The phase angle of the $m=2$ Fourier component of the latter is shifted with respect to that of the old underlying disc and therefore tends to decrease the normalized $m=2$ amplitude of the combined discs. The velocities, which are assigned to the new stellar disc component, follow the velocity distribu-

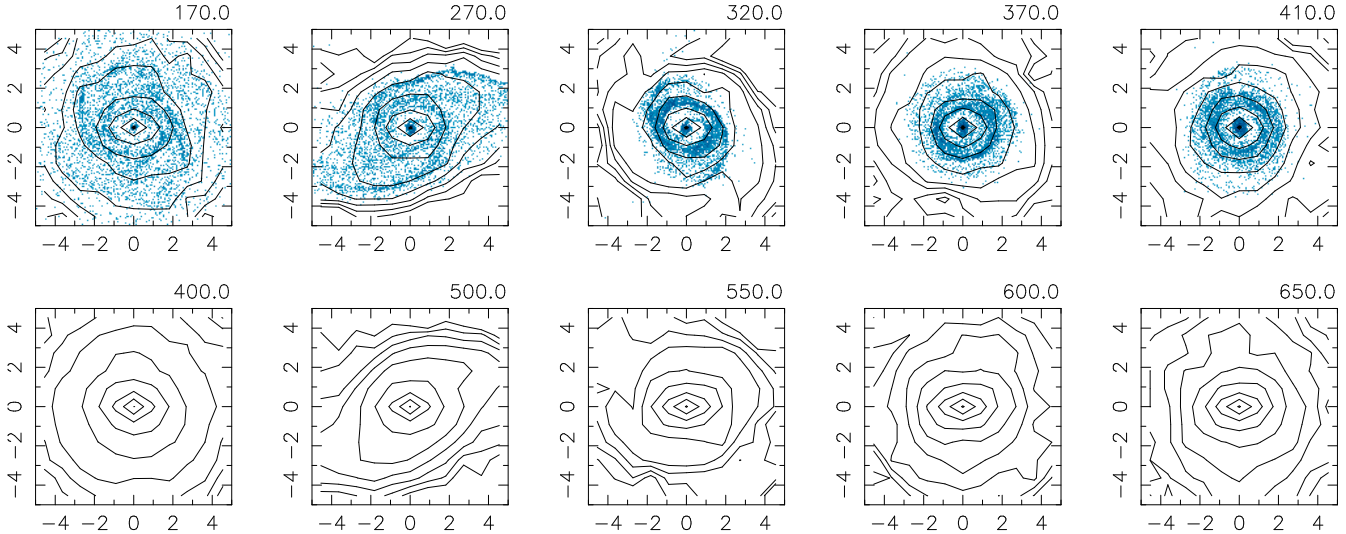


Figure 4. Examples of the morphological evolution of interaction models with and without gas. We show the face-on isodensity contours of the stellar disc for the models I0 C4 p (with gas, upper panels) and I1 C4 p (without gas, lower panels). For the first model a grey-scale plot of the gas particle distribution is shown. The layout is as for Fig. 1.

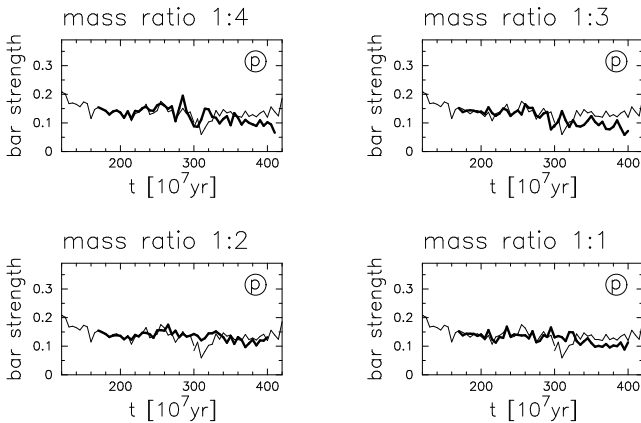


Figure 5. Evolution of the bar strength as a function of time for prograde, parabolic encounters with host galaxy I0 (thick line). The pericentric separation is $R_{\text{peri}}=15$ and the mass ratio $M_{\text{host}}:M_{\text{comp}}$ is given on top of each frame. The type of the companion's orbit is given in the upper right corner of each frame. For comparison we also show the bar strength of the isolated model (thin line).

tion of the *old* underlying stellar disc. Therefore the stellar disc of model I1 is initially slightly out of virial equilibrium, since the dispersion of the stellar particles is higher than that of the gas particles. After some $\Delta t=30$, however, the disc settles to a new equilibrium and the bar strength increases again, reaching its previous value and remaining constant after the short relaxation phase. Owing to the decreasing central mass concentration of the new stellar component, the pattern speed of the bar slightly decreases first, but remains roughly constant after the relaxation phase at about $\Omega_p=0.22\tau^{-1}$, or $21.5 \text{ km s}^{-1} \text{ kpc}^{-1}$, till the end of the run.

To gain some insight in the orbital structure of the disc of model I1, we locate the main planar periodic orbits in a frozen potential that rotates with the bar. General infor-

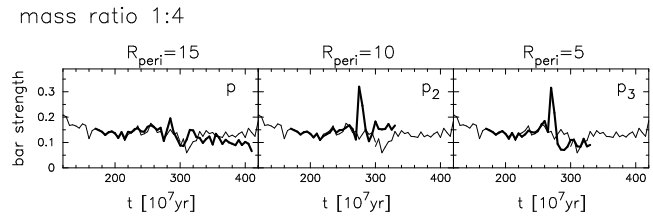


Figure 6. Same as Fig. 5, but for encounters with a fixed mass ratio of 1:4 and pericentric separations of 15 (p), 10 (p₂) and 5 (p₃), respectively.

mation on orbits in barred potentials can be found, e.g., in Contopoulos & Grosbøl (1989). The gravitational potential has been calculated the same way as described in the previous section, but is time-averaged over roughly one bar rotation. For simplicity, we restrict ourselves to planar orbits which are bi-symmetric with respect to the bar and close after one orbit around the centre in the frame of reference corotating with the bar. The results are then displayed in terms of a characteristic diagram, where for each orbit we plot its Jacobi integral E_J with respect to the y -intercept value with the $x=0$ plane. The Jacobi integral is a conserved quantity along any given orbit in the rotating frame, and can be thought of as an effective energy (e.g., Binney & Tremaine 1987). In the characteristic diagram the orbits form curves of families. In Fig. 3 we show the characteristic diagram of the main orbit families, using the notation of Contopoulos & Papayannopoulos (1980), in model I1 at the end of the run ($t=600$). The dashed curve is the zero-velocity curve (hereafter ZVC), which delineates the accessible region in the plane based on energy considerations. The family labelled x_1 consists of orbits that are elongated along the bar and predominately gives the bar its structure. Orbits of the x_2 -family are elongated perpendicular to the bar. Their presence is indicative of an ILR (or more than one) in the non-linear regime. The x_4 orbits are retrograde

Table 2. Notation of the interaction models.

R_{peri}	ω_{peri}			para- bolic
	0.3	0.6	0.9	
15.0	a	b	c	p
10.0	d	e	f	p1
5.0	g	h	i	p2

and slightly elongated perpendicular to the bar. The corotation radius in model I1 is at $E_J = -0.79$, or approximately 7.98 kpc. The x_2 -orbits range in energy from $E_J = -1.35$ to -1.07 , with semi-major axes ranging from 0.86 to 2.1 kpc.

5 INTERACTING MODELS WITH GAS

In this section we describe the simulations in which the gas-rich host galaxy I0 is perturbed by encounters with companions of different mass. The time of pericentric separation has been chosen to be $t_{\text{peri}} = 270$ for all runs with the host galaxy I0. In the first set of simulations the companions are initially set up to follow prograde, parabolic orbits with a pericentric separation of $R_{\text{peri}} = 15$, which is just outside the halo of the host galaxy. When referring to a specific model, we will hereafter use a notation like, for instance, ‘I0 C4 p’, where ‘I0’ is the name of the host galaxy, ‘C4’ is the name of the companion (see Tab. 1), and ‘p’ (parabolic) denotes the type of orbit, the latter following the notation given in Tab. 2. In Tab. 3 we summarise the basic parameters and properties of both the isolated and the interaction models. The first and the second column give the name of the host and of the companion galaxy, respectively, and the third column gives the orbit of the companion (see Tab. 2). In the fourth column we give the time when the companion is included in the simulation, resulting from the initial backward orbit integration (see Sec. 2.2). The fifth to seventh column give the pericentric separation and frequency, and the eccentricity of the orbit, respectively. In the eighth and ninth column we give the strength and pattern speed of the bar, respectively, after the interaction. The tenth and eleventh columns give the ratio of bar strength and pattern speed to the corresponding values of the isolated model. In the penultimate column we give the interaction strength parameter as defined in Sec. 6.1 and in the last column the corotation radius at the end of each run, determined from the linear analysis.

In Fig. 4 (upper panels) we show an example of the morphological evolution of the disc during an encounter, in this case for model I0 C4 p. The bar strength as a function of time for the models with different massive companions is shown in Fig. 5. We find that the encounters in this set of simulations are not sufficiently strong to regenerate the stellar bar in the disc, even for a mass ratio of 1:4, i.e. even with companion C4. In order to increase the strength of the tidal perturbation on the host galaxy, we run two additional simulations with companion C4, in which we now choose pericentric separations of $R_{\text{peri}} = 10$ and 5. The orbits of the companion are again chosen to be prograde and parabolic. The bar strength for these models is shown in Fig. 6. The peaks immediately following t_{peri} result from the time when the transient tidal arms contribute to the $m=2$ power in the

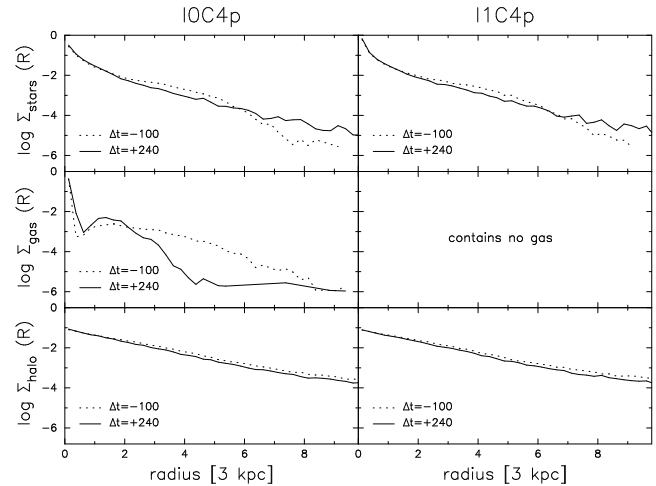


Figure 7. Logarithmic surface density as a function of radius for the stellar and gaseous disc and of the halo (from top to bottom, respectively). We show $\log \Sigma(R)$ for models I0 C4 p (left-hand panels) and I1 C4 p (right-hand panels). The dotted and full lines represent times before ($\Delta t = -100$) and after ($\Delta t = 240$) the interaction, respectively.

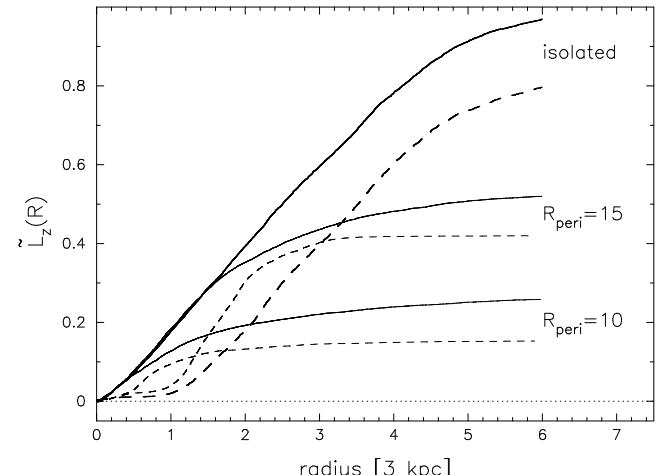


Figure 8. Specific cumulative angular momentum \tilde{L}_z as a function of radius in the stellar disc at the end of the run of the isolated model I0 (with gas) and of the interaction models with a mass ratio of 1:4 and different pericentric separations. The full and dashed lines show the results for the stellar and gaseous disc, respectively.

inner disc region, in which the bar amplitude is measured, but disappear as soon as the tidal arm features have dissolved. Even with these close encounters, it is not possible to regenerate the stellar bar in the disc of the gas-rich host galaxy.

In order to facilitate comparison with the purely stellar simulations described in the next section, we present here a more detailed analysis of the interaction simulations with the gas-rich host galaxy I0. As can be seen in Fig. 4 already, the interaction apparently leads to a significant redistribution of both the stellar and the gaseous material in the disc. This becomes more evident in Fig. 7, in which we show the

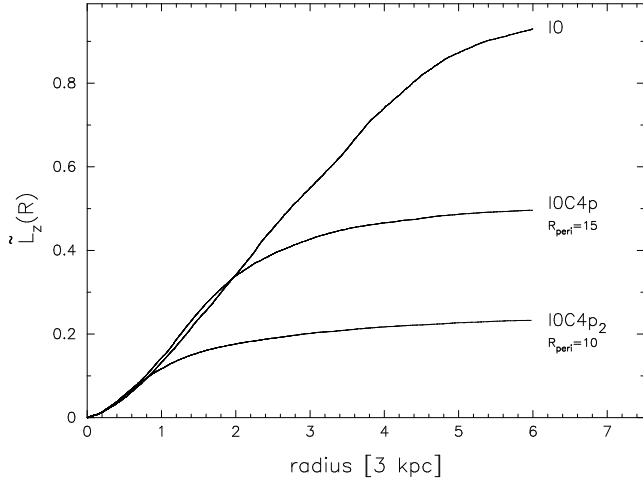


Figure 9. Same as Fig. 8, but for the combined disc (stars+gas).

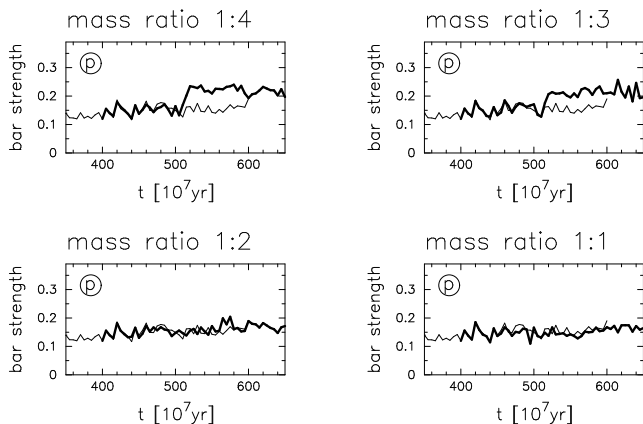


Figure 10. Bar strength as a function of time for the prograde, parabolic encounters with the purely stellar model I1 (thick line). The layout is as in Fig. 5.

logarithmic radial surface density of the disc and the halo for model I0 C4 p at times before and after the interaction. While the stellar density remains basically constant within a radius of approximately $R < 2.0$, i.e. roughly inside corotation in the corresponding isolated model, there is some net inflow of gas from the outer disc. The inflowing gas first piles up at a radius of about $R \approx 1.25$, which is close to the position of the gaseous ring, and then flows gradually towards the central disc region, accumulating in the nuclear disc. At the end of the run, the gas mass within 0.5 length units has increased by about 0.5 per cent of the total host mass, or some 6 per cent of the total gas mass, while the gas mass within 2 length units increased by roughly 1 per cent of the total mass, or about 12 per cent of the total gas mass. Some fraction of both the stellar and the gaseous material in the outer disc moves further out, contributing to the transient tidal arms and/or getting stripped off by the companion. The halo material in the inner region does not show any net radial redistribution, but we find some expansion in the outer parts, where halo material is also stripped off by the companion.

We measure also the specific cumulative angular mo-

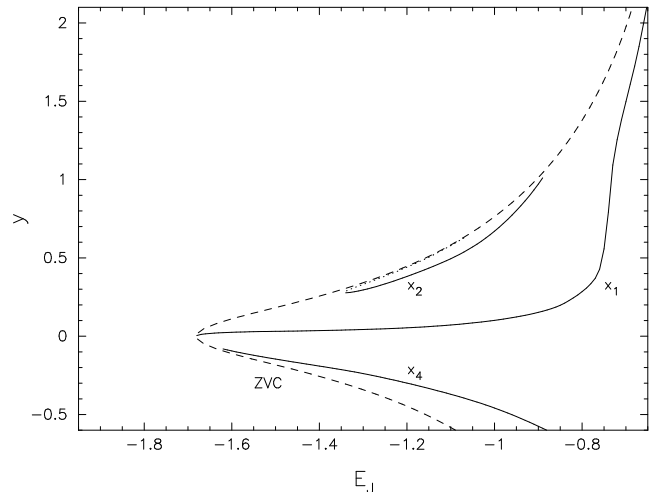


Figure 11. Characteristic diagram of model I1 C4 p after the interaction. The layout is as in Fig. 3.

mentum (hereafter \tilde{L}_z) as a function of radius for both the stellar and the gaseous disc, given by

$$\tilde{L}_z(R) = \left(\sum_{R_i < R} l_{z,i} \right) \times \left(\sum_{R_i < R} m_i \right)^{-1}, \quad (3)$$

where R_i , m_i and $l_{z,i}$ are the planar radius, the mass and the angular momentum, respectively, of the i -th disc particle. As an example we show in Fig. 8 the results of simulations with companion C4 and different pericentric separations. As can be seen in this plot, the interaction removes angular momentum from the stellar disc at all radii shown. We do not find any indication that the corotation radius of the bar or of the companion separates regions which gain from regions which lose angular momentum. More angular momentum is removed from the stellar disc for the closer pericentric separation. The gaseous disc shows a different behaviour. The gas in the inner disc gains angular momentum compared to the isolated model, within roughly $R = 3.0$ and 1.7 for pericentric separations of $R_{\text{peri}} = 15$ and 10 , respectively, and loses angular momentum outside those radii.

In Fig. 9 we show the specific cumulative angular momentum as a function of radius in the combined disc (stars+gas). We find that the disc in the interaction models I0 C4 p and I0 C4 p₂ does not lose, or even gains, angular momentum within a radius of $R \approx 2.0$ and $R \approx 1.0$, respectively, as compared to the isolated model I0.

6 INTERACTING MODELS WITHOUT GAS

In this section we describe the set of simulations with the purely stellar model I1 as the host galaxy. We start with simulations having similar orbits for the interaction as the ones described in the previous section, i.e. prograde and parabolic encounters using different companions (see Tab. 3). As shown in Fig. 10, in which we plot the bar strength as a function of time, simulations with mass ratios of 1:3 and 1:4 are, contrary to the dissipative models, sufficiently strong to regenerate the stellar bar in the disc,

Table 3. Main model parameters and properties.

Host	Comp	orbit	t_{start}	R_{peri}	ω_{peri}	e	$A_{(m=2)}$	Ω_p	$A/A_{I0,I1}$	$\Omega_p/\Omega_{I0,I1}$	Θ	CR
I0	–	–	0.0	0.14	0.30	1.0	1.0	...	2.05
I1	–	–	100.0	0.16	0.22	1.0	1.0	...	2.76
I0	C1	p	170.0	15.0	0.049	1.00	0.10	0.30	0.73	1.33	1.927	1.80
I0	C2	p	170.0	15.0	0.060	1.00	0.13	0.30	0.91	1.01	3.159	2.13
I0	C3	p	170.0	15.0	0.069	1.00	0.08	0.27	0.61	0.92	4.116	2.31
I0	C4	p	170.0	15.0	0.077	1.00	0.11	0.26	0.77	0.87	4.922	2.47
		p2	170.0	10.0	0.141	1.00	0.16	0.18	1.19	0.63		2.99
		p3	170.0	5.0	0.400	1.00	0.10	0.22	0.70	0.74		...
I0	C4	d	250.0	10.0	0.300	8.00	0.06	0.28	0.44	0.93	1.906	2.20
I1	C5	g	450.0	5.0	0.300	3.22	0.18	0.20	1.14	0.90	0.717	2.94
I1	C6	j	470.0	7.5	0.300	11.66	0.17	0.21	1.08	0.92	0.419	2.94
I1	C6	g	450.0	5.0	0.300	2.75	0.21	0.19	1.31	0.82	1.105	2.78
I1	C1	p	400.0	15.0	0.049	1.00	0.16	0.22	1.00	0.98	1.927	2.87
I1	C1	d	480.0	10.0	0.300	21.50	0.17	0.21	1.11	0.93	0.458	2.95
I1	C1	e	490.0	10.0	0.600	89.00	0.16	0.21	1.04	0.95	0.261	2.90
I1	C1	g	440.0	5.0	0.300	1.81	0.27	0.12	1.74	0.56	2.417	4.13
I1	C1	h	480.0	5.0	0.600	10.25	0.22	0.18	1.38	0.82	1.124	3.25
I1	C1	i	480.0	5.0	0.900	24.31	0.19	0.19	1.19	0.87	0.833	3.20
I1	C1	j	470.0	7.5	0.300	8.48	0.21	0.19	1.33	0.84	0.852	3.19
I1	C2	p	400.0	15.0	0.060	1.00	0.17	0.21	1.08	0.94	3.159	2.95
I1	C2	d	480.0	10.0	0.300	14.00	0.18	0.20	1.15	0.92	0.928	2.99
I1	C2	e	490.0	10.0	0.600	59.00	0.17	0.21	1.09	0.95	0.523	2.90
I1	C2	h	480.0	5.0	0.600	6.50	0.21	0.18	1.33	0.81	2.303	3.27
I1	C2	i	480.0	5.0	0.900	15.88	0.20	0.19	1.25	0.87	1.679	3.10
I1	C3	p	400.0	15.0	0.069	1.00	0.21	0.18	1.36	0.81	4.116	3.30
I1	C3	a	480.0	15.0	0.300	36.97	0.17	0.21	1.05	0.94	0.500	2.86
I1	C3	d	480.0	10.0	0.300	10.25	0.21	0.18	1.36	0.82	1.410	3.29
I1	C3	e	490.0	10.0	0.600	44.00	0.19	0.20	1.18	0.89	0.787	3.07
I1	C3	f	490.0	10.0	0.900	100.25	0.17	0.20	1.09	0.94	0.594	2.91
I1	C3	h	480.0	5.0	0.600	4.63	0.26	0.13	1.64	0.61	3.545	3.71
I1	C3	i	480.0	5.0	0.900	11.66	0.24	0.17	1.51	0.74	2.541	3.35
I1	C4	p	400.0	15.0	0.077	1.00	0.23	0.17	1.45	0.77	4.922	3.43
I1	C4	a	480.0	15.0	0.300	29.38	0.17	0.21	1.09	0.94	0.803	2.93
I1	C4	b	490.0	15.0	0.600	120.50	0.16	0.21	1.05	0.95	0.460	2.88
I1	C4	c	490.0	15.0	0.900	272.38	0.16	0.22	1.03	0.97	0.349	2.82
I1	C4	d	480.0	10.0	0.300	8.00	0.24	0.17	1.52	0.74	1.906	3.51
I1	C4	e	490.0	10.0	0.600	35.00	0.17	0.20	1.11	0.90	1.052	3.05
I1	C4	f	490.0	10.0	0.900	80.00	0.17	0.21	1.10	0.93	0.793	2.94
I1	C4	h	470.0	5.0	0.600	3.50	0.22	0.13	1.41	0.57	4.869	3.66
I1	C4	i	480.0	5.0	0.900	9.13	0.24	0.16	1.50	0.70	3.419	3.41

and the strength of the induced bar increases with the mass of the companion. In Fig. 11 we show as an example the characteristic diagram of the host galaxy of the interaction model I1 C4 p at time $t=640$, i.e. the end of the run, in which the stellar bar has been successfully regenerated by the interaction. The orbit analysis has been performed following the description given in Sec. 4. The corotation radius in this model is at $E_J = -0.63$, or about 10.3 kpc. The x_2 orbits range in energy from $E_J = -1.34$ to -0.88 , with semi-major axes ranging from 0.83 to 3.04 kpc.

Motivated by these results, we now explore a much wider – though still far from complete – parameter range, in order to determine the initial conditions necessary (or sufficient) to regenerate the stellar bar in the disc. We therefore run a set of simulations, in which we vary the orbit of the

companion, the pericentric separation R_{peri} and the mass M_C , respectively. The simulations and their basic initial parameters are summarised in Tab. 3. From the solution of the corresponding two-body problem the eccentricity e of the companions orbit has been determined by its angular frequency ω_{peri} at pericentre, and we restrict ourselves in this work to unbound orbits only. We choose ω_{peri} such that a prescribed number of inner Lindblad resonances is present in the disc, i.e. that certain orbits in the disc are in resonance with the companion, when passing R_{peri} .¹ Since the stellar bar in the unperturbed host galaxy is very weak, we

¹ We point out that the angular frequency of the companion, and therefore also the location of the corresponding resonances in the disc, changes with time.

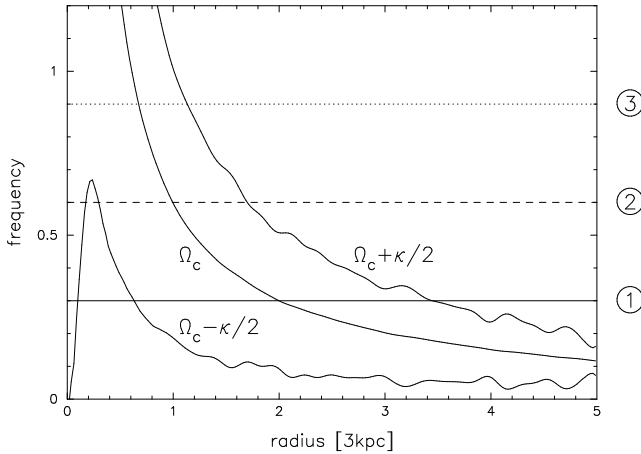


Figure 12. Basic frequencies of the isolated model I1 ($t = 500$) as a function of radius, obtained with the linear axisymmetric definition, using the epicyclic approximation. The horizontal lines mark the angular frequency ω_{peri} of the companion at the time of pericentric separation.

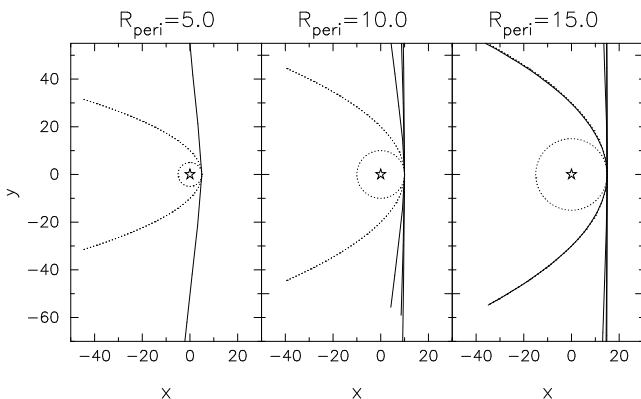


Figure 13. Different trajectories of the companion galaxy C4. We show the parabolic and hyperbolic orbits (full lines) from simulations with different pericentric separations, as given on top of each panel. The corresponding circular and parabolic orbits are indicated by dotted lines. The host galaxy is marked by a star in each panel.

apply the linear approximation, as described in Sec. 3, in order to determine the resonances in the disc. The resonance diagram for the isolated model I1 is shown in Fig. 12, and the frequencies chosen for the companion are:

1. $\omega_{\text{peri}} = 0.3$ (two ILRs)
2. $\omega_{\text{peri}} = 0.6$ (one ILR)
3. $\omega_{\text{peri}} = 0.9$ (no ILR) .

The mass of the companion for these simulations has been varied, as before, from 1:1 to 1:4, and we have a few additional runs with even lower mass ratios, namely 1: $\frac{1}{2}$ (C6) and 1: $\frac{1}{3}$ (C5). A complete list of all simulations and of their main parameters is given in Tab. 3. Some of the companion orbits are illustrated in Fig. 13 for different eccentricities and pericentric separations.

In Fig. 14 we show the bar strength as a function of time for this set of interaction models. It is striking that

– in contrast to the models with gas – the interaction is sufficiently strong to regenerate the bar in about half our models. As can also be seen from the plot, there is a general trend, that the strength of the induced bar increases with

- increasing mass M_C of the companion,
- decreasing pericentric separation R_{peri} ,
- decreasing pericentric frequency ω_{peri} .

This is what one might generally expect, since the gravitational force of the companion is proportional to its mass, the tidal force decreases with R^{-3} , and the time integrated force of the companion on the host galaxy becomes stronger for slower passages.

Furthermore, after the bar has formed in the disc, we find that the amplitude of the bar stays constant with time. We have checked the life-time of the regenerated bar by running model I1 C4 d, which shows a significant increase in bar strength after the interaction, for roughly $\Delta t = 4 \times 10^{10}$ yr in total. Using a linear-fitting we find a decay-rate of the bar of roughly 9×10^{-12} yr. With this the bar will drop to half its amplitude after approximately $\Delta t = 5 \times 10^{10}$ yr. After one Hubble time (with $H_0^{-1} = 1.3 \times 10^{10}$ yr) the bar amplitude would have dropped only by 12 per cent. A fraction of this decrease could be introduced by the relatively low number of particles used in the simulations, so that in fact there could be (almost) no sign of a decay for bars formed in interactions. These results strongly argue for the fact that bars formed by the interaction are long-living and by no means transient phenomena.

6.1 Dynamical properties of the bars

To quantify the correlations described in the previous section, we define a parameter Θ , which allows us to evaluate the interaction strength:

$$\Theta \equiv \left\langle \frac{f_{\text{comp}}}{f_{\text{gal}}} \right\rangle = \int \frac{f_{\text{comp}}}{f_{\text{gal}}} dt, \quad (4)$$

where f_{gal} and f_{comp} are the mean radial forces, exerted from the host I1 and the companion galaxy, respectively, averaged over the equatorial plane of the host galaxy. In practice we calculate them on a radial equally-spaced polar grid with maximum radius $R = 4.8$ and then take a density weighted average. The integral in eq. (4) is carried out from $t = -250$ to $t = 250$, with $t = 0$ corresponding to t_{peri} , in order to guarantee an adequate convergence of Θ in all models. For these force calculations both galaxies are approximated by point masses for simplicity. The results for Θ are given in the penultimate column of Tab. 3. We also calculate the normalized bar strength A/A_{I1} , where A and A_{I1} are the bar strength in the interaction model and in the isolated model, respectively. By plotting the normalized bar strength versus the interaction strength parameter Θ (Fig. 15), we find a roughly linear correlation between the two quantities for each companion C_i , with $i = 1 \dots 4$. One of the 1 : 4 models (I1 C4 h) is systematically off-set in all plots of this kind (i.e., Figures 15, 17 and 19), but always lies within the 2σ confidence limit. The models with parabolic encounters are all off-set from the relationships found, but seem to be correlated themselves linearly.

Plotting the bar strength of the different models in a diagram showing the logarithmic orbital eccentricity e versus

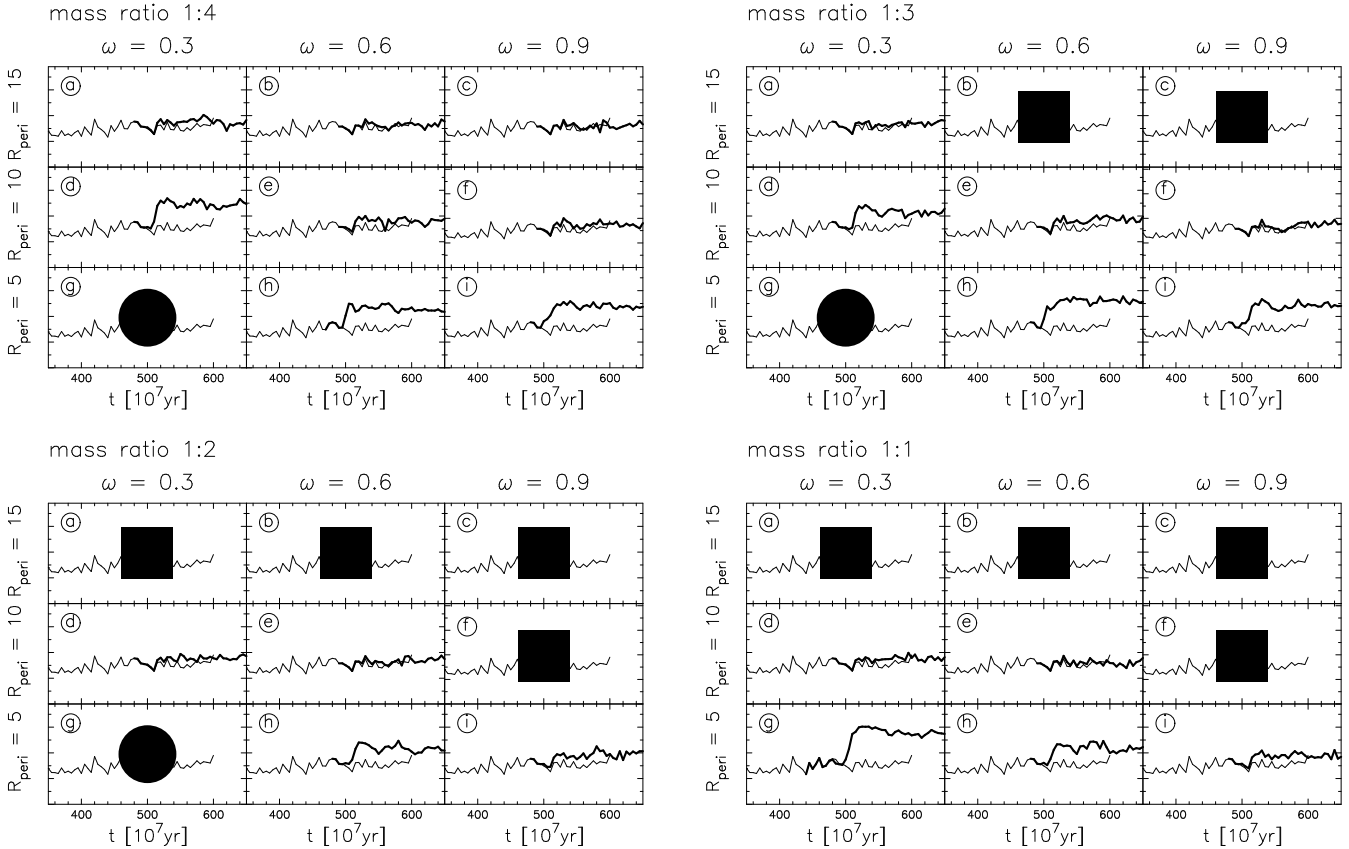


Figure 14. Bar strength as a function of time for some of the pure stellar models. The four frames show the models with mass ratios of 1:1, 1:2, 1:3 and 1:4, respectively. The filled squares mark models which have not been run, because other runs allow us to deduce that a bar cannot form. Models in which the companion would be on a bound elliptical orbit are marked by a filled circle.

the angular frequency ω_{peri} (see Fig. 16), we find that models with orbits of roughly $\log e > 1.2$ are not sufficiently strong to regenerate the bar in the purely stellar models. A larger sample of simulations has to be run, however, to confirm the existence of such a limiting eccentricity. If such a limit really exists, it would give a necessary, but not sufficient condition for tidally induced bar formation for our purely stellar model.

Angular momentum exchange in isolated galaxies leads to correlations between the bar pattern speed and strength, as well as between the bar strength and the angular momentum gained by the spheroid, which, in many cases, is a measure of the angular momentum exchanged (Athanassoula 2003). We will now test whether such correlations can be found in our regenerated bars. We indeed find a tight correlation between the strength and the pattern speed of the regenerated bars (Fig. 17). The stronger the bar gets after the interaction, the lower becomes its pattern speed, in good agreement with Athanassoula (2003). We further find that the pattern speed in the interaction models is always lower than in the corresponding isolated case.

The passage of the companion again is accompanied by a redistribution of disc angular momentum. The angular momentum exchange between the different disc regions (as defined in the previous section) is similar to that in Fig. 8. In Fig. 18 we show the radial distribution of the specific cu-

mulative angular momentum $\tilde{L}_z(R)$ for a set of simulations with companion C4 in comparison with the isolated model I1. For the runs with lower mass companions, we find similar results. It is noticeable that the regeneration of the stellar bar has been feasible only in those models which show a significant change in \tilde{L}_z . Actually we find a tight correlation between the loss of angular momentum ΔL_z in the disc measured inside the initial disc cut-off radius r_{cut} and the induced bar strength, as shown in Fig. 19. The more angular momentum is removed from the disc, the stronger the regenerated bar becomes, in good agreement with what was found for isolated bars by Athanassoula (2003). We find the same correlation about equally strong when we plot the angular momentum change within the corotation radius. This important connection between the angular momentum exchange and the (re)generation process of the bar is described further in the discussion section.

7 DISCUSSION

The regeneration of stellar bars triggered by galaxy interactions has been suggested as an additional scenario for the formation of bars and for explaining the observed frequency of bars along the Hubble sequence (Sellwood & Moore 1999 ; Friedli 1999; Athanassoula 2000). So far only the formation of tidally induced bars in initially non-barred disc galaxies

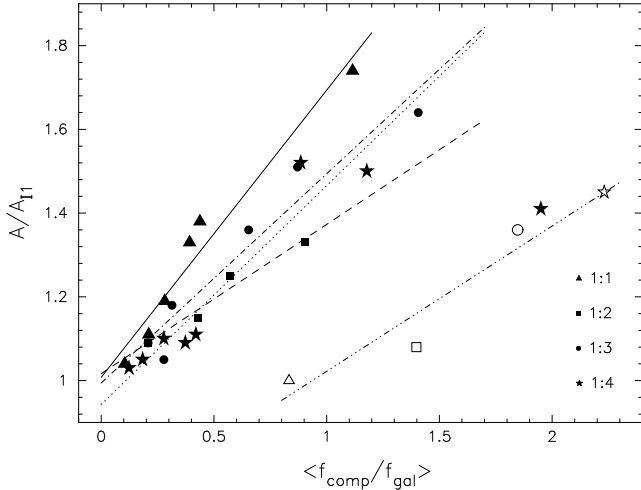


Figure 15. Normalized bar strength A/A_{I1} versus the interaction strength parameter Θ . We show the results of the purely stellar simulations and the corresponding linear fits for mass ratios of 1:1 (bullets, full line), 1:2 (squares, dashed line), 1:3 (triangles, dotted-dashed line) and 1:4 (stars, dotted line). The simulations with parabolic orbits are shown with open symbols and are not taken into account for the linear fits.

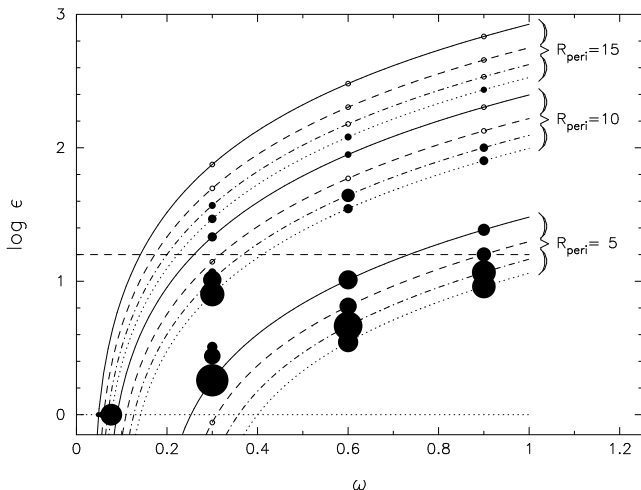


Figure 16. Logarithmic orbital eccentricity versus the angular frequency of the companion at pericentre time. For each pericentric separation the curves obtained from the corresponding two-body problem are plotted for different mass ratios: 1:1 (full line), 1:2 (dashed), 1:3 (dotted-dashed) and 1:4 (dotted line). The filled circles mark the different simulations and their size is proportional to the bar strength at the end of each run. The two circles which do not lie on a line are simulations with mass ratios of 1:0.5 and 1:0.33. The limit of ϵ , as explained in the text, is marked by the horizontal dashed line.

and the required conditions, under which such an event may occur, have widely been studied by means of numerical simulations (Byrd et al. 1986; Noguchi 1988; Salo 1991; Miwa & Noguchi 1998; etc.). These results, however, need not necessarily apply to interactions with a *formerly* barred galaxy. Indeed, a former stellar bar likely might have changed the dynamics of the disc, i.e. increased the velocity dispersion in the stellar disc and changed both the density and angular

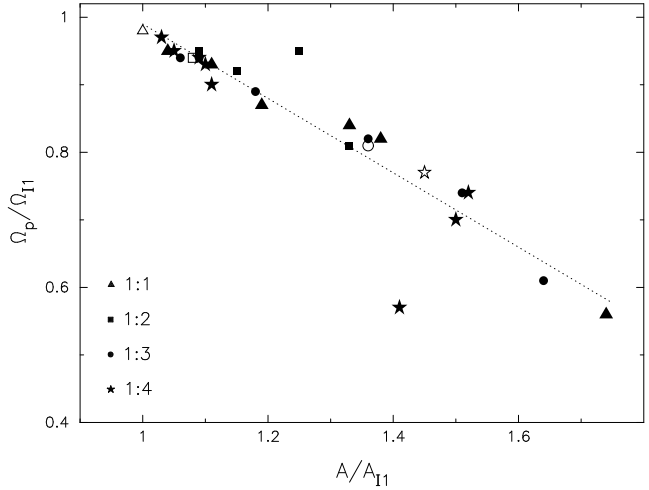


Figure 17. Normalized pattern speed Ω_p/Ω_{I1} versus normalized bar strength A/A_{I1} of the purely stellar interaction models. Symbols are as in Fig. 15.

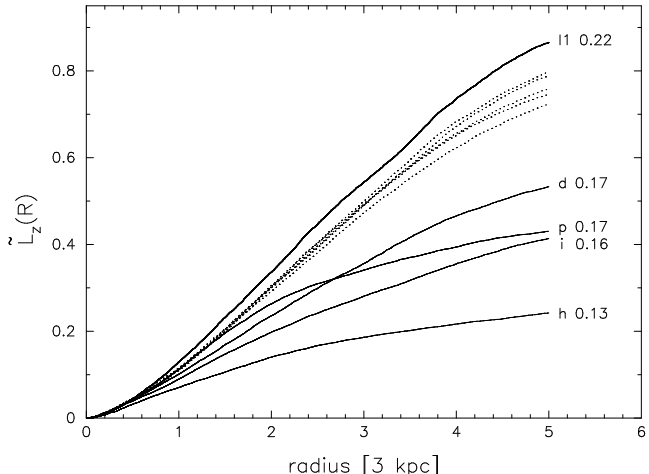


Figure 18. Specific cumulative angular momentum of the stellar disc for the isolated model I1 (thick line) and different interaction models I1C4 (thin lines). The dotted lines indicate models in which no or only a weak increase of bar strength has been found after the interaction. Models in which the bar has been regenerated (full lines) are labelled (with the orbit type as given in Tab. 3) and the corresponding bar pattern speed is given.

momentum distribution (compare Fig. 20). Therefore, the regeneration of stellar bars is subject to different conditions than the formation of a bar in an bar-unstable isolated disc or in a tidal interaction.

In this work we present numerical simulations starting with a host galaxy which has initially been bar unstable and in which the bar has been significantly weakened due to gas inflow before the interaction.

7.1 Quantifying the interaction strength

To quantify the strength of the interaction, we have introduced a parameter Θ for the interaction strength (Sec. 6.1), which basically takes the following quantities into account: 1) the mass of the companion, 2) the pericentric separation

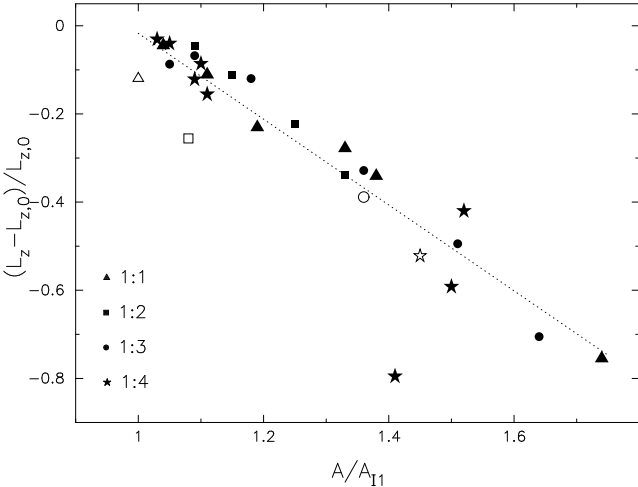


Figure 19. Total change of angular momentum ΔL_z of the stellar disc inside its initial cut-off radius as a function of bar strength normalized by the corresponding value of the isolated model. The different symbols represent interactions with different mass ratios. Parabolic and hyperbolic orbits are represented by open and filled symbols, respectively.

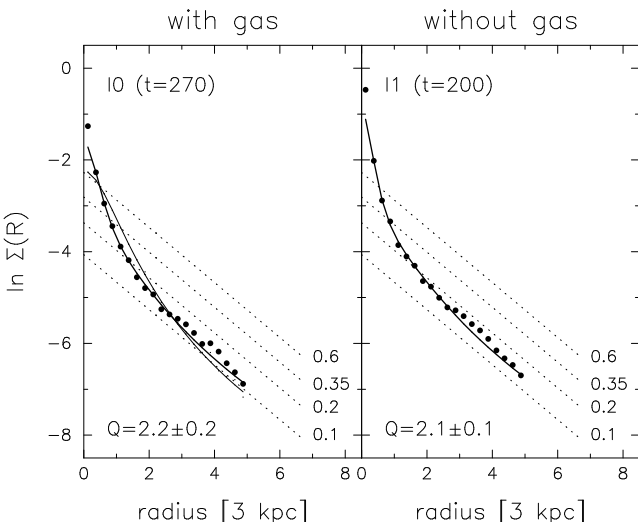


Figure 20. Logarithmic surface density of the stellar disc of models I0 (left-hand panel) and I1 (right-hand panel). The filled dots show the density distribution of the stellar discs and the thick full lines the best-fit of the corresponding Kuzmin-Toomre profile. The thin full line in the left-hand panel gives the density distribution of the initial stellar disc in model I0. We also show the different exponential discs used by Miwa & Noguchi (1998) with dotted lines and give the mass of each disc in their model units. The value of the Toomre Q-parameter of the stellar disc is given at the bottom of each panel.

between the galaxies, and 3) the velocity of the companion at pericentre, defining a kind of interaction time-scale. With our definition (see Sec. 6.1), we find that the interaction strength Θ correlates well, i.e. roughly linearly, with the strength of the regenerated bars, which have been created in our purely stellar models.

A different parameter for the interaction strength has

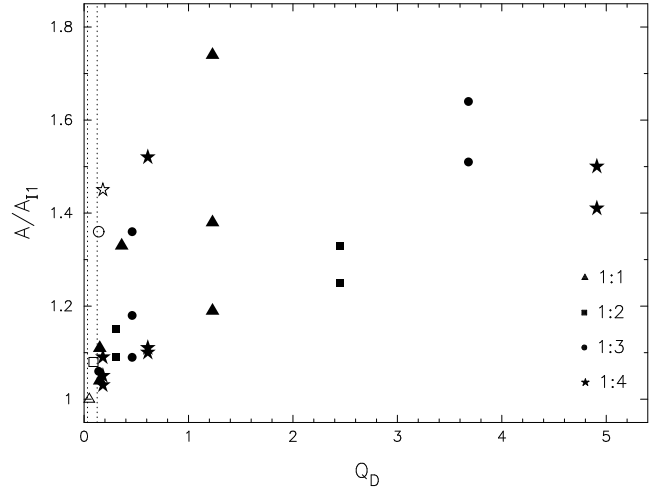


Figure 21. Normalized bar strength A/A_{I1} versus the Dahari index Q_D (Dahari 1984) for interactions with different mass ratios. The layout is as in Fig. 15.

been introduced by Dahari (1984) as an estimate of the direct tidal impulse:

$$Q_D = (M_{\text{comp}}/M_{\text{host}})/(R_{\text{min}}/R_{\text{disc}})^3, \quad (5)$$

where M_{comp} and R_{peri} are the mass of the companion galaxy and the pericentric separation, respectively. M_{host} is the mass of the host galaxy within the disc truncation radius R_{disc} . Salo (1991) has used the Dahari index as a quantitative measure for tidally induced bar formation in his 2D simulations and found a minimum value of Q_D , depending on the specific host galaxy, above which a bar is formed by the interaction. The specific limiting value of Q_D Salo found depends strongly on the central mass concentration of the host galaxy and cannot be easily transferred to our model. Furthermore, applying the Dahari index to our simulations we find neither a correlation between the strength of the interaction and the regeneration of the bar, nor a limiting value of Q_D (see Fig. 21). The main drawback of the Dahari index is that it does not take into account the interaction orbit, i.e. the interaction time-scale. The Dahari index therefore does not seem to be sufficient to constrain the parameters necessary for the formation or regeneration of bars by galaxy interactions in general.

A more advanced parameter has been introduced by Elmegreen et al. (1991). This is based on the Dahari index, but includes also the ratio between an interaction time-scale ΔT and some dynamical time T of the disc:

$$Q_E = Q_D \times \frac{\Delta T}{T}, \quad (6)$$

where $T = R_{\text{gal}}^3/GM_{\text{gal}}$ and ΔT is the time it takes the companion to move by one radian relative to the host's centre at pericentre time. These authors also report a limiting value $Q_E = 0.038$ for the formation of the bar by tidal interactions. Applying this parameter to our simulations we find a correlation between the interaction strength and the strength of the regenerated bar (see Fig. 22). This, however, is less pronounced than the corresponding one for our parameter Θ , which takes more fully the interaction into account. The existence of a limiting parameter, as found by Salo (1991)

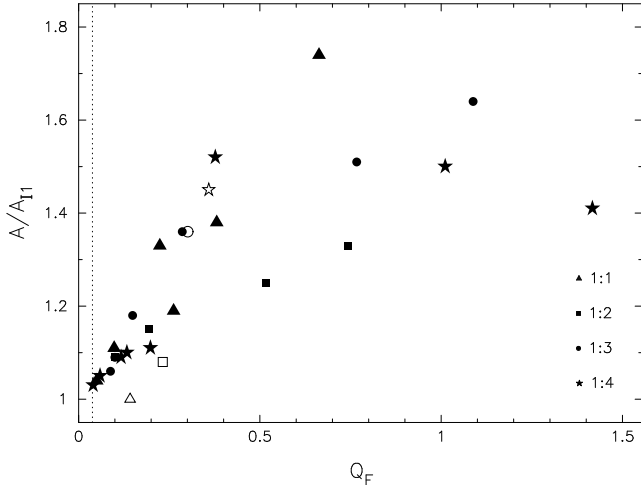


Figure 22. Normalized bar strength versus the interaction parameter Q_E (Elmegreen et al. 1991). The layout is as in Fig. 15.

and Elmegreen et al. (1991), however, might be attributed to the method for measuring the bar strength. For our purely stellar simulations we find a correlation between Θ and the induced bar strength rather than a limiting value of Θ . Still, the exact correlation between Θ and the bar strength – as described in Sec. 6.1 – is likely to be model dependent.

7.2 Radial redistribution of angular momentum

Athanassoula (2003) argued that the redistribution of angular momentum is the driving agent for the evolution of an isolated barred galaxy. Both her analytical work and her numerical simulations show that galaxies that have exchanged more angular momentum should have a stronger bar, with a faster decreasing pattern speed. In our purely stellar models, we also find that, whenever bar regeneration occurs, it is always accompanied by a considerable loss of angular momentum from the disc (see Fig. 18). Indeed, as in the case of isolated galaxies (Athanassoula 2003), there is a tight correlation between the strength of the bar and the angular momentum lost by the inner disc. This argues that angular momentum exchange is tightly linked to the bar formation process, independent of whether that is spontaneous, or driven.

The actual exchange process, however, is not always the same. In isolated discs angular momentum is emitted by particles in resonance with the bar in the inner part of the disc (within corotation), and, to a lesser extent and if there is a considerable bar growth, by non-resonant particles in that region. This is absorbed by particles in the outer disc and halo. In this case there is only one pattern speed, that of the bar, since the spirals, which could in principle have a different pattern speed (Tagger et al. 1987; Sygnet et al. 1988), have died away in the early parts of the simulations. Thus resonances are well defined. This is certainly not the case here. Besides the bar pattern speed, there is the driving frequency of the interaction which changes with time. Furthermore, the forcing from the companion is of comparable strength to that of the bar, and the companion itself participates actively in the angular momentum exchange. Thus, in contrast to the isolated cases, we do not find the bar coro-

tation radius to separate disc angular momentum emitters from disc absorbers.

The bar regeneration process can be understood in terms of basically the same angular momentum considerations as described by Athanassoula (2003) for isolated disc galaxies. The bar in an isolated disc can get stronger and lose angular momentum basically by four different effects, which should be linked to each other. First, particles which were on quasi-circular orbits outside the bar get trapped into elongated orbits in its outer part and thus the bar becomes longer. Secondly, the orbits trapped in the bar could get thinner and make the bar thinner, too. Third, more mass could be get trapped on periodic orbits in the bar. And finally, the bar can of course lose angular momentum by slowing down. These effects should also be present in our case as well, where the loss of disc angular momentum is predominantly driven by the tidal perturbation of the companion. We will discuss here how much the different effects contribute to the regeneration of the stellar bars in our simulations. Since analytical calculations cannot make any statements about this, we will base the discussion on the dynamical properties and orbital structure of our specific models.

In Fig. 23 (right-hand column, upper panel) we show a direct comparison of the characteristic diagrams of the purely stellar models I1 and I1 C4 p at the end of each run, respectively. The characteristic diagram of the isolated and the perturbed case look very similar in terms of the layout of the main periodic orbits. The main difference, however, is that both the x_1 and the x_2 orbits extend to higher energies after the interaction. This is especially obvious for the part of the x_1 characteristic around $E_J = -0.75$, where the value of the y intercept increases strongly with E_J . This clearly moved towards higher energies. In Fig. 24 (right-hand column) we show some examples of the periodic orbits with different Jacobian energies E_J of both the x_1 and the x_2 family. We find that the x_1 orbits become longer and, to some smaller extent though, also thinner after the interaction. This becomes clearer in Fig. 23 (middle panel), in which we plot the axial ratio b/a of the orbits, where a and b denote the major and minor axis, respectively, as a function of E_J . The main effect, however, is the lengthening of both the x_1 and the x_2 orbits towards higher energies and, taking into account the corresponding characteristic diagram, also in radial extent. For the x_1 orbits we also notice some lengthening towards lower energies, as well. Owing to these effects the bar gets both more centrally concentrated and more extended to large radii.

The thinning of the periodic orbits, which is less pronounced in our models than the lengthening, can be understood by the analytic calculations by Lynden-Bell (1979; hereafter LB79) in the context of gradual bar growth in isolated disc galaxies. As described in LB79, the mean circular frequency Ω_c of most disc stars in the central and/or inner disc region is much higher than the pattern speed Ω_p of the weak periodic perturbation, which is considered to be bar-like in this case. In the frame of reference corotating with the perturbation, the fast motion $\Omega_c - \Omega_p$ of the stars on near-circular orbits is not considerably affected by the weak perturbation and therefore the fast action variable J_f (see LB79) is approximately constant. As shown by Lynden-Bell, angular momentum is removed from the orbits, whose elongation leads the perturbing bar-like potential. Near-resonant

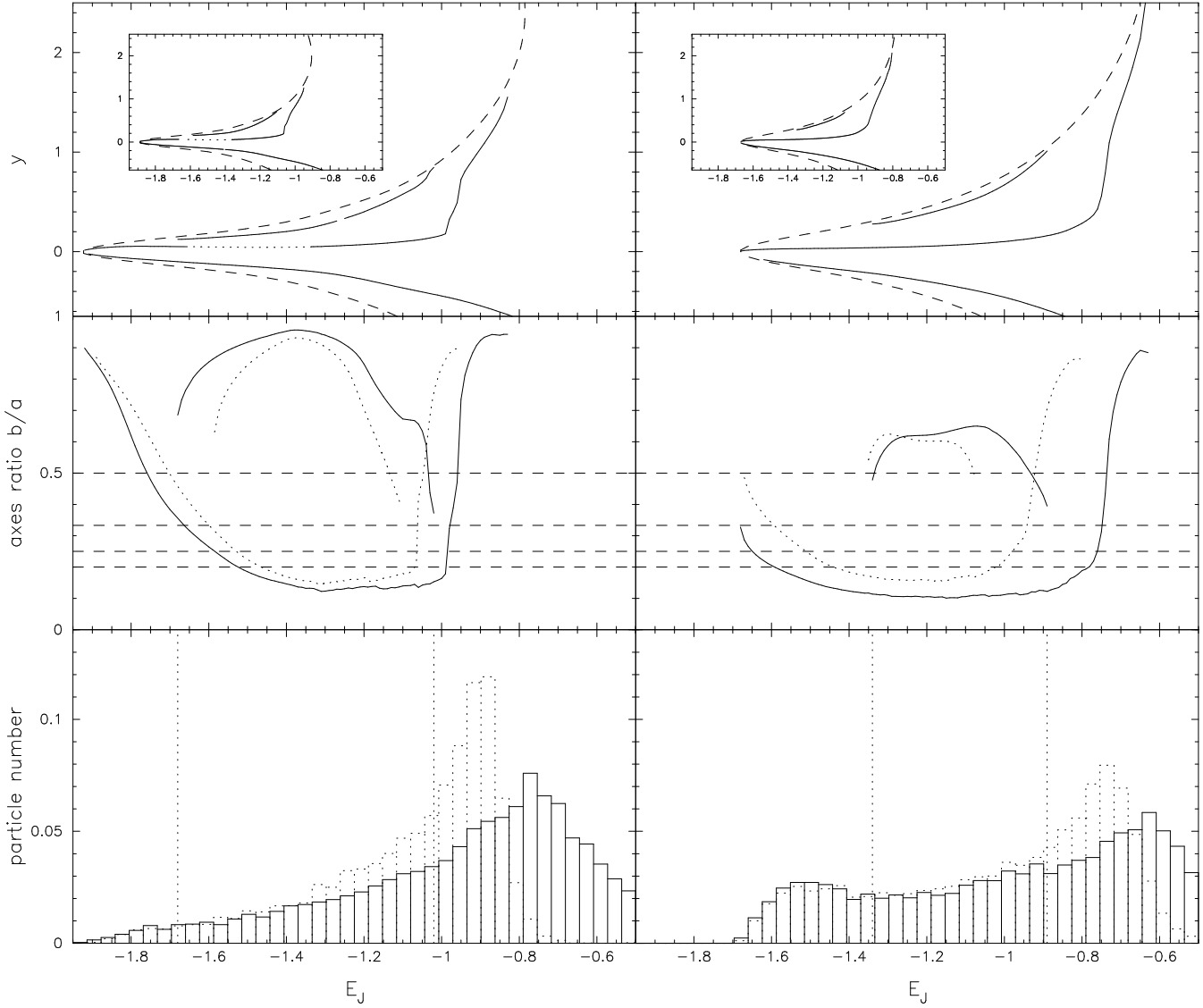


Figure 23. Comparison of models I0 C4 p (with gas; left-hand side) and I1 C4 p (without gas; right-hand side). The upper panels show the characteristic diagram at the end of the run of the interaction model (main panel) and of the corresponding isolated model (subpanel). The layout of the diagrams is the same as for, e.g., Fig. 3. Instability regions in the characteristic curves are indicated by dotted lines. In the middle panels we show the axial ratios b/a of the x_1 and x_2 orbit families, where a and b are the major and minor axis, respectively. The full and dotted lines show the results of the interaction and the isolated model, respectively. The horizontal dashed lines indicate axes ratios of 1:2, 1:3, 1:4 and 1:5. The bottom panels show a histogram of the number of stellar disc particles within corotation per energy interval, normalized by total number of stellar disc particles within corotation in the corresponding isolated model. The vertical dotted lines mark the region in which the x_2 orbits is present in the perturbed models.

orbits in the inner disc region, which reside in the abnormal region (see Fig. 2 in LB79), i.e. the region where $\Omega_i = \Omega_c - \frac{1}{2}\kappa$ of the orbit decreases as its angular momentum decreases with constant J_f , will align with the perturbation and become more eccentric, supporting the growth of the bar structure. As pointed out by Lynden-Bell, this way the bar shape also becomes more eccentric, but the length of the bar will not change significantly. The main difference to the scenario described in LB79 is that in our case, the perturbation is not periodic, since it is due to both the companion and the bar, and the angular frequency of the former is a function of time.

We finally check which orbits are important for making the bar. In the lower panel of Fig. 23 we therefore plot the number of particles as a function of E_J , normalized by the total disc particle number within corotation of the isolated model I1. This way we get information about how the principal orbits at different energies are populated in our model. As can be seen from this plot, the total number of stellar particles within the corotation radius increased by less than 10 per cent. We conclude that the mass of the bar does not increase significantly. The main effect we find is that particles with energies close to the vertical x_1 -branch move

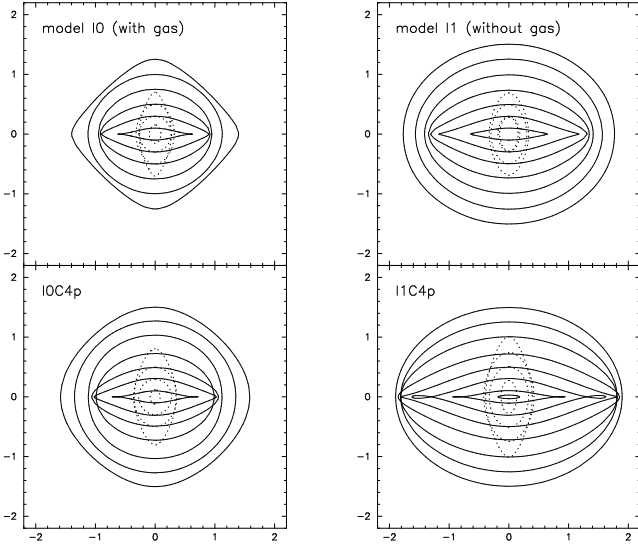


Figure 24. Concentric orbits of the x_1 (full lines) and x_2 (dotted lines) families. The left- and the right-hand column show the models with and without gas, respectively. In the upper panels we show the isolated models I0 and I1 and in the lower panels models I0 C4 p and I1 C4 p.

towards higher energies or higher radial extent, taking into account the characteristic diagram.

By tracking individual particle orbits in the corresponding potential and plotting their average y-intercept versus the Jacobian energy E_J in the characteristic diagram, we find that the x_2 orbits in the purely stellar models are only populated by a very small fraction of particles. This result is consistent with Fig. 25, in which we show the surfaces of section of model I1 C4 p at the end of the run for different E_J . As can be clearly seen, the x_1 family dominates phase space over a wide range in energy and the x_2 orbits are almost not present.

7.3 Influence of the gas

Interactions which are strong enough to induce a bar in our purely stellar models are not sufficiently strong to induce a bar in the N -body/SPH models. In fact it has not been possible to induce a bar in any of our dissipative models, and we will here discuss the possible reasons for this. The stellar disc component in these simulations loses angular momentum, as was found also in the purely N -body models (see Fig. 8 and 18). The gas in the inner parts, however, gains angular momentum, so that the inner parts of the disc may gain a small amount of angular momentum (see Fig. 9), or if they lose, it is considerably less than the corresponding quantity for the purely stellar case. Furthermore, as was shown in Fig. 7 the interaction is accompanied by a significant inflow of gas towards the central disc. These two effects, coupled, prevent the regeneration of the bar. In this section we discuss how the increase of the central mass concentration affects the orbital structure of the disc and thus helps prevent the regeneration of the bar in these models.

In Fig. 23 (left-hand column) we compare models with gas, before and after the interaction. In particular, for models I0 and I0 C4 p, we compare the characteristic diagrams

(upper panel), the axial ratio of the x_1 and x_2 orbits (middle panel) and the particle number per energy range (bottom panel). In contrast to the models without gas (right column) the characteristic diagram of the models with gas extends more to lower energies, as would be expected from Fig. 7 and Sec. 4, that show clearly that the density distribution is centrally more concentrated in models with gas. Furthermore, the extent of the x_2 orbits is considerably larger, and the x_1 orbits have a sizeable instability strip between roughly $E_J = -1.34$ and -1.66 .

Information on the axial ratio of the x_1 and x_2 orbits and on their extent is given in the middle panels of Fig. 23 and in Fig. 24. We see clearly that the differences between the cases before and after the interaction are much smaller than for the purely stellar case. The x_1 orbits are a bit thinner after the interaction and the x_2 orbits have slightly larger radial extent, but the differences are small. From Fig. 23 and 24 we see that the x_1 orbits are less elongated than the corresponding orbits in the models without gas. This is particularly true at the highest and lowest energies. The extent of the elongated orbits is also considerably shorter. Also the x_2 orbits in the central region, i.e. at lower energies, are much rounder in the case with gas.

The number of stellar particles within corotation in models with gas (Fig. 23; bottom panel) have increased by roughly 12 per cent compared to the corresponding isolated model. Particles move from the intermediate energy region to the high energy one, and also, though to a lesser amount, to the low energy central region, similar to what is found in the models without gas.

Comparing the SOSs of models with and without gas (I0 C4 p and I1 C4 p, respectively) after the interaction (Fig. 25), we note that the area corresponding to x_1 orbits is much smaller in models with gas. On the other hand the area corresponding to chaotic motion and the area corresponding to x_2 orbits is considerably larger. The chaos in the cases with gas is due to the instabilities of the x_1 orbits, discussed above. The larger area covered by the x_2 orbits is in agreement with the fact that the x_2 characteristic is much more extended. To pursue this further we followed in the frozen potential the orbits of particles with initial conditions from the simulation, as we had already done for the simulations without gas. We find a notable difference. Namely there is now an indication that, contrary to the purely stellar case, a non-negligible fraction of the orbits is trapped around x_2 orbits. This difference can be understood as a result of the induced gas-inflow (see Fig. 7), in accordance with the results found in numerical simulations of isolated gas-rich barred galaxies (e.g., Friedli & Benz 1993; Berentzen et al. 1998). Owing to the growing central mass concentration the x_2 orbits cover a larger phase-space volume at the expense of the x_1 orbits.

Thus the fact that bars cannot be regenerated in simulations with gas can be understood with the help of the many differences between the two models, described above. There is considerably less angular momentum loss from the inner disc material, if this is not a gain. The interaction brings considerably less change of the shape and extent of the x_1 orbits, but renders them unstable over a considerable energy interval, thus introducing a considerable amount of chaos. Finally, due to the increased central concentration, the importance of the x_2 population is considerably increased. The

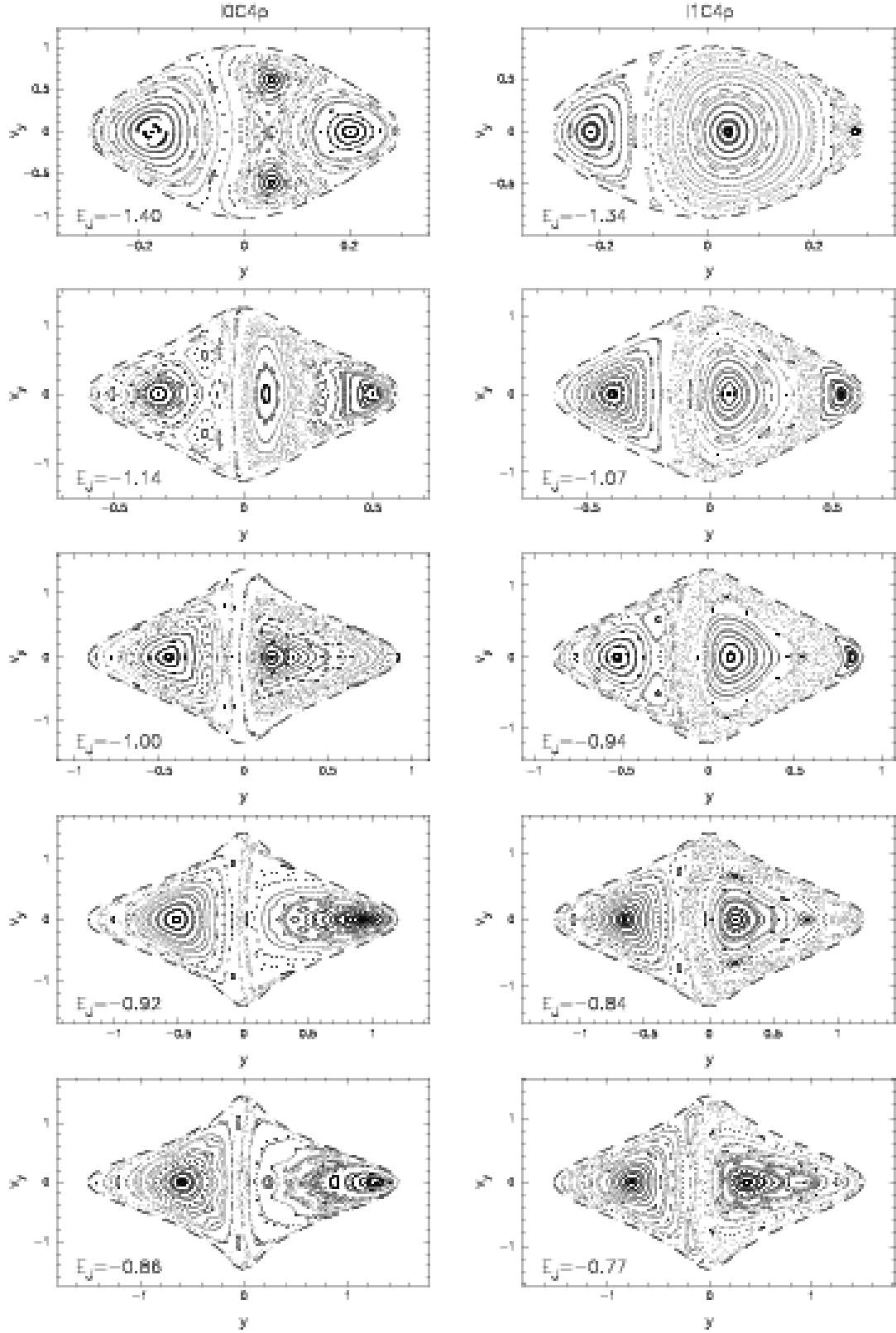


Figure 25. Surfaces of section for models I0 C4 p (with gas; left-hand column) and I1 C4 p (without gas; right-hand column) at the end of the runs. The values of the Jacobian energy E_J , given in the bottom left corner of each panel, have been chosen such as to give roughly the same range in y for each row. In the purely stellar model the phase space is dominated by the x_1 and x_4 orbits at low Jacobian energies, while in the models with gas the phase space is mainly dominated by the x_2 and irregular orbits.

coupling of these three anti-bar effects prevents the regeneration of a bar component.

7.4 Properties of regenerated bars

As a next step we discuss the properties of the regenerated bars compared to the ones formed by the bar instability in isolated discs. Contrary to Miwa & Noguchi (1998), we find no clear evidence for qualitative differences between the two types of bars, while we do find clear evidence for similarities. The orbital differences between the two types of bars, discussed in the two previous subsections are quantitative, rather than qualitative, since they pertain only to the extent of the families and the shape of the corresponding orbits. The role of the resonances seems the same.

Athanassoula (2003) found a correlation between the bar strength and the pattern speed of bars in isolated disc galaxies. In order to compare the properties of the bars formed in our models and the ones in isolated discs, we first calibrate our model units appropriately, as proposed in Athanassoula & Misiriotis (2002), and then compared them to the ones in Athanassoula (2003). The result is shown in Fig. 26, which shows that the area covered by the driven bars is not separated by that covered by the isolated bars. This argues strongly for the similarity between the dynamical properties of the two types of bars, and the difficulty to distinguish between them.

Elmegreen & Elmegreen (1985) found two different types of major axis surface density profiles, the exponential and the flat ones, and Noguchi (1996) argued that this distinction could be due to the fact that the first type is found in spontaneous bars and the second in driven ones. We believe that the difference is due to the bar strength, rather than its origin, since Athanassoula & Misiriotis (2002) showed that both types of profiles could be found in isolated galaxies: the flat profiles occurring in the stronger bars and the exponential ones in less strong ones.

Apart from these differences, we find agreement with the results of Miwa & Noguchi (1998). Thus, in our purely stellar simulations we find a roughly linear correlation between the pattern speed of the regenerated bar and its strength, or, accordingly, the interaction parameter Θ (see Fig. 17 and 15, respectively). In other words, stronger bars – regenerated by the interaction – have lower pattern speeds. This result is in agreement with the simulations of Miwa & Noguchi (1998), who find a similar correlation – less strict though – between the pattern speed of the induced bars and the companions mass. In both cases, i.e. the formation (Miwa & Noguchi 1998) and regeneration of stellar bars (see Fig. 17) by tidal interactions, the bars always have lower pattern speeds than the bars formed spontaneously in the corresponding isolated models.

In agreement with Noguchi (1987) and Gerin et al. (1990) we find that tidal bars are not transient, but long-lived, as are spontaneous bars. Thus bars which are observed at high redshifts (Sheth et al. 2003) may have formed by galaxy interactions and thus played an important role in the evolution of disc galaxies (Sheth et al. 2003).

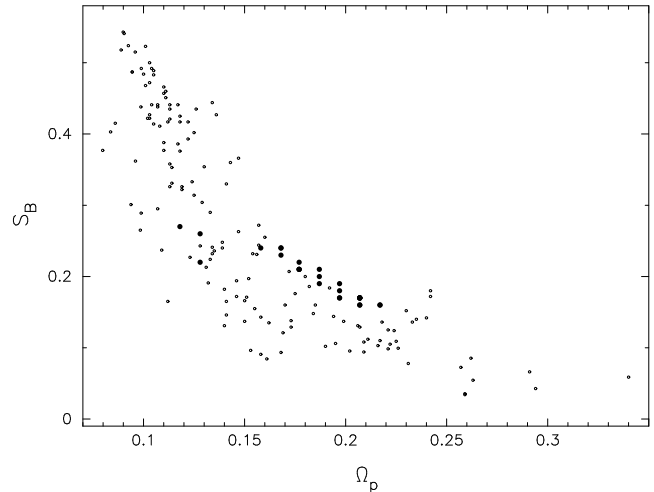


Figure 26. Bar strength S_B versus pattern speed Ω_p in units used by Athanassoula & Misiriotis (2002). The dots and bullets show the results of the isolated models of Athanassoula (2003) and our purely stellar interaction models, respectively.

7.5 Numerical considerations

The simulations presented in this work have been performed with a rather low particle number of the host galaxy, because of the relatively large sample of simulations. On the one hand the induced numerical noise in general supports the bar formation process, while on the other it will heat the disc, and thus make the bar regeneration more difficult. We trust, however, that a higher number of particles would make only quantitative, and not qualitative differences. Thus the physical results should remain unchanged.

The companion galaxy in our simulations has always been approximated by a softened point mass. For simulations in which the companion passes outside the halo of the host galaxy, this approximation is well suited. For simulations in which the companion crosses the halo, however, dynamical friction can be sufficiently strong to change the orbit of the companion and finally lead to a merger between the two galaxies.

8 SUMMARY

In this paper we used numerical simulations to investigate the regeneration of a stellar bar by tidal encounters. The host galaxy has been chosen to be initially bar unstable and forms a large-scale bar during its early evolution. Before the interaction with the companion galaxy the bar significantly weakened, owing to the bar-driven gas-inflow towards the central disc region. For the simulations presented in this work we used two different types of host galaxies, i.e. one gas-rich disc model and one without gas. The encounters in our simulations have been chosen to be prograde with respect to the rotation in the host disc and co-planar with the discs equatorial plane. The mass and the orbit of the companion have been varied in order to cover a large parameter space.

We found that interactions, which are sufficiently strong to regenerate the bar in the purely stellar models, do not lead to a regeneration in the dissipative models. The regenerated

bars in our simulations are long-living phenomena and by no means only transient, i.e. that (regenerated) bars formed by interactions may indeed contribute to the number of barred spirals at high redshifts and in the local Universe.

We have shown that the strength of the regenerated bars increases with the interaction strength. Owing to the tidal perturbation, angular momentum is removed from the disc. In fact, the whole disc within its initial cut-off radius loses angular momentum, in contrast to what is found for isolated discs, where the corotation radius of the bar separates disc regions losing and gaining angular momentum. The amount of angular momentum removed from the disc shows a clear correlation with the interaction strength. We argued that the main effect of this angular momentum loss is a significant extension of the region where bar-supporting orbits exist, resulting in a lengthening of the bar. As a further, though somewhat less important, effect, we found also a thinning of both the bar-supporting orbits and the bar itself.

The regenerated bars have lower pattern speeds than the bars in the corresponding isolated models. Furthermore, we found strong correlation between the strength and the pattern speed of the bar. This correlation is in very good agreement with the correlation found for bars in isolated discs. This is one of the pieces of evidence that the regenerated bars are qualitatively similar to those formed in isolated discs and thus cannot easily (if at all) be distinguished from them by their dynamical properties.

In contrast to the purely stellar simulations presented in this work, it has not been possible to regenerate the bar in our models including gas. We argued that this is due to the fact that less angular momentum is lost from the inner disc and to the fact that, owing to the interaction, additional gas is driven towards the centre of the disc. We concluded that the regeneration of stellar bars by galaxy interactions seems to be a reasonable mechanism for galaxies containing not too much gas, provided the external forcing is sufficiently strong.

9 ACKNOWLEDGMENTS

We would like to thank Albert Bosma for interesting discussions, J.C. Lambert and C. Theis for their computer assistance, and the referee, Ron Buta, for his comments.

I.B. acknowledges support from DFG grant Fr 325/48-2, /48-3 and Volkswagen Foundation grant I/76520. He thanks the DFG for funding the grape facilities at the Sternwarte Göttingen. C.H. acknowledges support from grants HST-AR-09546.02-A, NSF-AST-0206251, GSU-FRG-2002, and DFG Fr 325/39-1, /39-2. E.A. would like to thank the IGRAP, the INSU/CNRS and the University of Aix-Marseille I for funds to develop the grape facilities used for part of the calculations in this paper. The final draft of this paper was written while E.A. was in I.N.A.O.E. She thanks the I.N.A.O.E. staff for their kind hospitality and ECOS-Nord/ANUIES for a travel grant that made this trip possible.

REFERENCES

Athanassoula E., 2000, review in the XIVth IAP meeting "Galaxy Dynamics, from the Early Universe to the Present"

Athanassoula E., 2002, *ApJ*, 569, L86

Athanassoula E., 2003, *MNRAS*, 341, 1179

Athanassoula E., Misiriotis A., 2002, *MNRAS*, 330, 35

Athanassoula E., Sellwood J.A., 1986, *MNRAS*, 221, 195

Barnes J.E., Hernquist L.E., 1991, *ApJ*, 370, 65

Berentzen I., Athanassoula E., Heller C.H., Fricke K.J., 2003, *MNRAS*, 341, 343

Berentzen I., Heller C.H., Shlosman I., Fricke K.J., 1998, *MNRAS*, 300, 49

Binney J., Tremaine S., 1987, *Galactic Dynamics*, Princeton Univ. Press, Princeton NJ

Bournaud F., Combes F., 2002, *A&A*, 392, 83

Byrd G.G., Valtonen M.J., Valtaoja L., Sundelius B., 1986, *A&A*, 166, 75

Contopoulos G., Grosbøl P., 1989, *A&ARv*, 1, 261

Contopoulos G., Papayannopoulos Th., 1980, *A&A*, 92, 33

Dahari O., 1984, *AJ*, 89, 966

de Vaucouleurs G., 1963, *ApJS*, 8, 31

Elmegreen B.G., Elmegreen D.M., 1985, *ApJ*, 288, 438

Elmegreen D. M., Sundin M., Sundelius B., Elmegreen B., 1991, *A&A*, 244, 52

Eskridge P.B., Frogel J.A., Pogge R.W., et al., 2000, *AJ*, 119, 536

Friedli D., 1999, in: *The evolution of galaxies on cosmological timescales*, eds. J.E. Beckman J.E., Mahoney T.J., ASP Conf. Series 187, 88

Friedli D., Benz W., 1993, *A&A*, 268, 65

Gerin M., Combes F., Athanassoula E., 1990, *A&A*, 230, 37

Heller C.H., 1991, Ph.D. thesis, Yale University

Heller C.H., Shlosman I., 1994, *ApJ*, 424, 84

Hohl F., 1971, *ApJ*, 168, 343

Kuzmin G., 1956, *Astron. Zh.*, 33, 27

Lynden-Bell D., 1979, *MNRAS*, 187, 101L

Lynden-Bell D., Kalnajs A.J., 1972, *MNRAS*, 157, 1L

Miller R.H., Prendergast K.H., Quirk W.J., 1970, *ApJ*, 161, 903

Miwa T., Noguchi M., 1998, *ApJ*, 499, 149

Monaghan J.J., 1992, *ARA&A*, 30, 543

Noguchi M., 1987, *MNRAS*, 228, 635

Noguchi M., 1988, *A&A*, 203, 259

Noguchi M., 1996, *ApJ*, 469, 605

Ostriker J.P., Peebles P.J.E., 1973, *ApJ*, 186, 467

Plummer H.C., 1911, *MNRAS*, 71, 460

Salo H., 1991, *A&A*, 243, 118

Sellwood J. A., 1981, *A&A*, 99, 362

Sellwood J. A., Moore E.M., 1999, *ApJ*, 510, 125

Sheth K., Regan M.W., Scoville N., Sparke L., 2003, *ApJL*, *in press*

Shlosman I., Frank J., Begelman M.C., 1989, *Nat*, 338, 45

Spitzer L., 1942, *ApJ*, 95, 329

Steinmetz M., 1996, *MNRAS*, 278, 1005

Sugimoto D., Chikada Y., Makino J., Ito T., Ebisuzaki T., Umemura M., 1990, *Nat*, 345, 33

Sygnat J.F., Tagger M., Athanassoula E., Pellat R., 1988, *MNRAS*, 232, 733

Tagger M., Sygnat J.F., Athanassoula E., Pellat R., 1987, *ApJ*, 318, 43L

Toomre A., 1963, *ApJ*, 138, 385